JOURNAL OF Materials CHEMISTRY

Oxygen content and microstructure in $Bi_4V_2O_{11-\delta}$

E. García-González, M. Arribas and J. M. González-Calbet*

Facultad de Químicas, Departamento de Química Inorgánica, Universidad Complutense, 28040 Madrid, Spain. E-mail: jgcalbet@eucmax.sim.ucm.es

Received 5th April 2001, Accepted 24th May 2001
First published as an Advance Article on the web 26th July 2001

Selected area electron diffraction and high resolution electron microscopy have been used to study the room temperature-stable polymorph of the $Bi_4V_2O_{10}$ phase. The reciprocal lattice, as well as the unit cell symmetry and the microstructural features, are in agreement with the $P22_12_1$ space group and a disordered distribution of anionic vacancies in the perovskite-type layers of the structure.

Introduction

Among the Aurivillius[1] oxides, the family $(Bi_2O_2)^{2+}(VO_{3.5x})^{2-}$ $(0<x<0.5)$ is of particular interest, owing to its ionic conductivity properties.[2] The fascinating conducting behavior of γ-$Bi_4V_2O_{11}$[3] has led to several attempts to stabilize such materials at room temperature by means of a doping strategy using different metallic ions. Such substitutions give rise to the so-called BIMEVOX family of materials.[4]

Most of the doping processes to stabilize the γ-polymorph led to compounds with oxygen contents lower than O_{11}. $Bi_4V_2O_{11}$ itself can be relatively easily reduced by modifying the thermal treatment and the oxygen partial pressure during the synthesis procedure. In this case, the production of a certain amount of V^{4+} can be considered as an *in situ* doping process. Galy *et al.* have reported the solid solution for $(Bi_2O_2)_2(V^{V}_{1-x}V^{IV}_{x})_2O_{11-x}$ $(0<x<1)$.[5] According to Joubert *et al.*,[6] however, the $V^{V}\rightarrow V^{IV}$ reduction process accounts only for one third of the V^{V} ions, thus leading to $Bi_4V_2O_{10.66}$ $(Bi_6V_3O_{16})$. This orthorhombic material[6] can also be considered as an Aurivillius phase, although isolated V_3O_{10} units constitute the V–O layers in which a VO_6 octahedron shares vertices with two VO_4 tetrahedra, leading to unconnected chains along the *b* axis. This fact is responsible for the insulating behavior of such materials. On the other hand, when only V^{IV} is present, the orthorhombic $Bi_4V_2O_{10}$ phase is formed.[5] According to the few reports on this material,[5,7,8] it seems to be a new Aurivillius oxide built up from $(Bi_2O_2)_n$ layers alternating with $(V_2O_6)_n$ layers formed by VO_5 square pyramids sharing vertices.

The average structural features of all these phases are already well established. Microstructural details of the O_{11} and $O_{10.66}$ phases, as well as the structural transformation between them, have been studied by Huvé *et al.*[9] using HREM and HT-TEM. However, little is known about the possible order–disorder states associated with the oxygen stoichiometry in $Bi_4V_2O_{10}$ and, in this sense, electron microscopy would provide a valuable insight.

A recently reported[7] study has shown an $\alpha\rightarrow\beta\rightarrow\gamma$ phase transition in the $680\,^{\circ}C<T<850\,^{\circ}C$ range, similar to the well-known transition which occurs in $Bi_4V_2O_{11}$. A preliminary study by means of electron diffraction[8] shows the α-polymorph to present a unit cell very similar to that of the $Bi_4V_2O_{10.66}$ phase, with a triple *b* axis with respect to the $n=1$ Aurivillius term. However, previous work on the O_{10} material[5] suggested a different unit cell metric for the room temperature-stable polymorph, where no superstructure along the *b* axis was found.

In light of these somewhat contradictory reports, we present in this paper a comparative study by selected area electron diffraction (SAED) and high resolution electron microscopy (HREM) of $Bi_4V_2O_{11-x}$, $0<x<1$, in order to establish the relationship between oxygen content and ordered distribution of the different vanadium environments.

Experimental

α-$Bi_4V_2O_{11}$ was prepared by heating stoichiometric amounts of Bi_2O_3 (Merck, 99.9%) and V_2O_5 (Merck, 99.9%) at 600 °C for 12 h and subsequent treatments at 700 °C for 12 h and 800 °C for 12 h in air. Then, the sample was fired at 800 °C for 6 h under oxygen flow to avoid the $V^{V}\rightarrow V^{IV}$ partial reduction. Finally, the product was slowly cooled (20 °C h^{-1}) to room temperature in the same atmosphere.

A CAHN-D200 electrobalance was used to prepare the reduced samples. $Bi_4V_2O_{10.66}$ was obtained by reduction of α-$Bi_4V_2O_{11}$ at 450 °C under 100 mbar H_2/400 mbar He, whereas $Bi_4V_2O_{10}$ was prepared by reduction at 650 °C under 200 mbar H_2/300 mbar He. The oxygen content of the samples was determined by both thermogravimetry and chemical analysis by titration after dilution in 3 M HCl with Mohr's Salt.

Powder X-ray diffraction (XRD) was performed on a Philips X'PERT diffractometer equipped with a bent copper monochromator and using Cu-Kα radiation.

SAED was carried out using a JEOL 2000FX electron microscope. HREM was performed with a JEOL 4000EX electron microscope. Samples were ultrasonically dispersed in n-butanol and transferred to carbon-coated copper grids.

Results and discussion

Powder XRD patterns of the three samples under study could be indexed on the basis of the orthorhombic unit cells previously reported for α-$Bi_4V_2O_{11}$,[10,11] $Bi_4V_2O_{10.66}$[6] and $Bi_4V_2O_{10}$.[5] The striking similarity between the three patterns hides the microstructural features accompanying the decrease in the oxygen content. For this reason, a SAED and HREM study was performed.

Fig. 1 shows the SAED patterns taken along the [001] and [100] projections for the $Bi_4V_2O_{10.66}$ material.† For the $Bi_4V_2O_{11}$ sample, two different type of crystals are observed. A few show the sixfold modulation along *b**, which is characteristic of the O_{11} nominal composition[10,11] (Fig. 2a), but the majority give the diffraction patterns displayed in

†Miller indices have been assigned corresponding to the basic unit cell of the $n=1$ Aurivillius term.

 DOI: 10.1039/b103126k

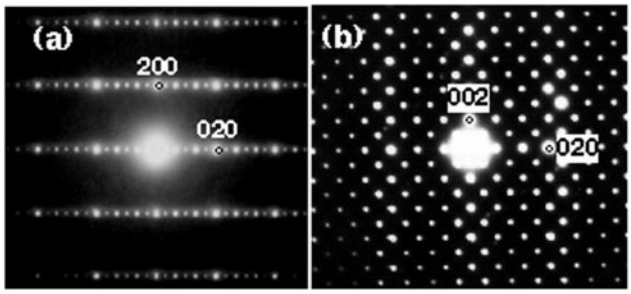

Fig. 1 SAED patterns for the $Bi_4V_2O_{10.66}$ phase taken along the (a) [001] and (b) [100] zone axes.

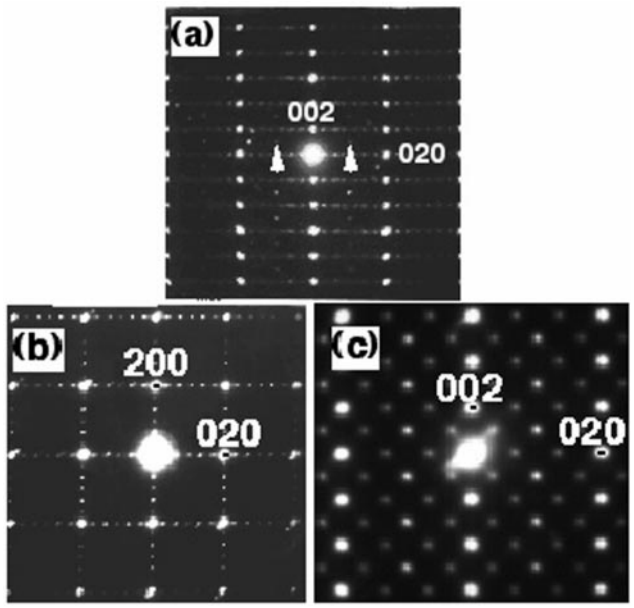

Fig. 2 (a) SAED pattern of the first type of crystals found in the $Bi_4V_2O_{11}$ material, taken along the [100] zone axis. The central spot, marked with an arrow, indicates the beginning of the reduction process under the electron beam. (b) and (c) SAED patterns showing the [001] and [100] reciprocal projections of the most common type of crystals found in $Bi_4V_2O_{11}$.

Fig. 2b and c along the [001] and [100] zone axes, respectively. The [001] projection shows a three-fold superstructure along both a^* and b^* reciprocal directions for the O_{11} composition. The same superstructure can be observed, only along one of the basal reciprocal directions, for the $O_{10.66}$ material (Fig. 1a). The presence of these extra diffraction maxima along b^* is a well known fact and it has been previously associated, in $Bi_4V_2O_{10.66}$,[9] to the ordered alternation of vanadium polyhedra along the corresponding lattice direction according to the $\cdots TOT'OT' \cdots$ sequence (T, T′ = tetrahedra; O = octahedra).

Fig. 3 shows the HREM images of $Bi_4V_2O_{10.66}$ and $Bi_4V_2O_{11}$ projected along the [100] direction. Crystals of the $Bi_4V_2O_{10.66}$ material (Fig. 3a and SAED pattern in Fig. 1b) are well ordered and homogeneous in contrast and show the characteristic regular and undulating black and white contrast alternation along the b axis,[9] attributed to the presence of isolated V_3O_{10} units which constitute the perovskite slabs, as well as the expected stacking sequence of the unit cell along c. The most common crystals in the $Bi_4V_2O_{11}$ material (Fig. 3b and SAED pattern in Fig. 2c), however, are not homogeneous in contrast but characterised by the disordered intergrowth of structural domains (the corresponding unit cells are marked in the figure). Careful examination of the contrast inside each domain shows the same sequence as in the $O_{10.66}$ material.

It is clear, from the previous statement, that the crystals with the nominal composition $Bi_4V_2O_{11}$ are composed of domains

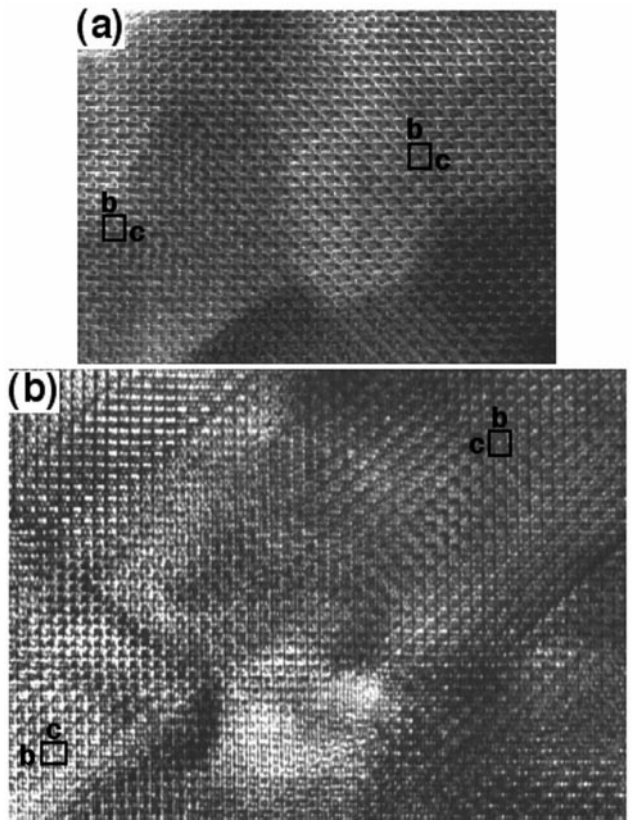

Fig. 3 (a) High resolution electron micrograph of $Bi_4V_2O_{10.66}$ projected along the [100] direction. (b) HREM image of $Bi_4V_2O_{11}$ taken along the [100] zone axis (corresponding SAED pattern shown in Fig. 2c).

of the $Bi_4V_2O_{10.66}$ phase. It is worth mentioning that attempts to take HREM images of the first type of crystals observed for the O_{11} sample (SAED pattern in Fig. 2a) led to their partial reduction and to the rapid disappearance of the six-fold modulation along b. However, the second type of crystals, discussed in the previous paragraph (Fig. 2b and c), are stable under the electron beam and did not show any change in either the diffraction pattern or the image contrast during the observation time. Provided that they constitute most of the bulk of the sample, and taking into account that the chemical analysis data are in agreement with the O_{11} anionic stoichiometry, we interpret the oxygen excess with respect to $Bi_4V_2O_{10.66}$ to be located in the domain walls.

From the above discussion, it seems reasonable to suppose that any attempt at oxidation from the $O_{10.66}$ nominal composition would be accommodated by means of microdomain formation, thus reinforcing the fact that the structure of $Bi_4V_2O_{10.66}$ seems to be the most stable disposition of the anionic vacancies in the $Bi_4V_2O_{11-\delta}$ system.

It is well known that the most important factor affecting the study of the $Bi_4V_2O_{11}$ structure is the facility of the $V^V \rightarrow V^{IV}$ reduction process. In the $Bi_4V^V_{2-x}V^{IV}_xO_{11-\delta}$ solid solution described by Galy *et al.*,[5] only the composition $\delta = 0.33$ shows a well-defined structure. The average structure of the $\delta = 1$ phase has been studied by single crystal XRD[5] and the total substitution of V^V by V^{IV} seems to lead to the formation of perovskite-type layers with V^{IV} in square pyramidal coordination sites. The authors observed the existence of three allotropic forms, named α, β and γ by analogy with the polymorphs of $Bi_4V_2O_{11}$, with transition temperatures of 680 and 850 °C. Subsequent structural characterization of $Bi_4V_2O_{10}$ has been reported by Satto *et al.*[8] by means of X-ray diffraction and electron microscopy on the low temperature form α-$Bi_4V_2O_{10}$. Based on their diffraction studies, the authors propose a unit cell clearly related to the $Bi_4V_2O_{10.66}$ phase with

the tripling of the b parameter compared to the γ-form. Our investigations on the reciprocal lattice of the O_{10} compound revealed, however, a $5 \times 5 \times 15$ Å metric for the unit cell, where no superstructure along b^* is observed.

At this point, is important to mention that the synthetic method employed here always leads to a variable amount of metallic bismuth together with the main reduction product, an Aurivillius-type phase. It is a well known fact[5,6] that the oxygen content variation allowed in $Bi_4V_2O_{11-\delta}$ ranges from $\delta = 0$ to $\delta = 1$. Electron diffraction studies on crystals with the Aurivillius-type structure show a reciprocal lattice consistent with the space group $P22_12_1$ which was previously proposed by Galy *et al.*,[6] for the O_{10} anionic composition. Taking into account the above information, together with the careful control of the reduction process and the corresponding weight loss as well as the comparison with the partial reduction to give $O_{10.66}$, leads to the assumption that the reduced sample is mainly composed of $Bi_4V_2O_{10}$.

Fig. 4 shows the SAED patterns of the reduced phase $Bi_4V_2O_{10}$ along the [100] and [$\bar{1}$10] zone axes. The systematic extintions observed in the reciprocal space would be in agreement with the orthorhombic space group $P22_12_1$ (no. 18), as has already been mentioned. The reciprocal space calculation using the atomic coordinates of space group $P22_12_1$ as input data led to the calculated diffraction patterns shown in Fig. 5 for the [100], [001] and [$\bar{1}$10] projections. The agreement between both calculated and experimental diagrams is clear. It is worth recalling that the [100] SAED pattern reported by Satto *et al.*,[8] does not agree with the calculated one and is identical to that obtained for the $Bi_4V_2O_{10.66}$ material. The presence of very weak (00l) maxima with $l = 2n + 1$ in the SAED pattern along [$\bar{1}$10] (see Fig. 4b), which are forbidden reflections for this space group, could be due to multiple diffraction because of the thickness of the crystal.

Fig. 6 shows a HREM image of $Bi_4V_2O_{10}$ on the [100] projection. Neither the presence of a three-fold superstructure along b nor the characteristic wavy contrast that would be expected in the light of the model proposed by Satto *et al.*[8] with an ordered distribution of square pyramids along b, is observed. It is worth emphasizing that this type of contrast is clearly observed in the $Bi_4V_2O_{10.66}$ phase (see Fig. 3a), which shows striking similarities. The calculated image[12] in the inset (simulation conditions: $\Delta f = -60$ nm, $t = 7.0$ nm), by using the atomic coordinates of space group $P22_12_1$ as input data, is in agreement with the alternation of Bi_2O_2 and V_2O_2 layers, the latter composed only of VO_2 pyramids randomly pointing up and down.

From the above discussion, it emerges that the unit cell found for the room temperature-stable polymorph is, therefore, that previously proposed for the γ-form with a disordered distribution of anionic vacancies in the perovskite-type layers of the structure.

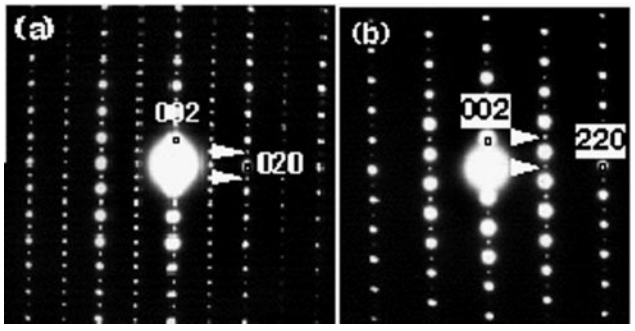

Fig. 4 SAED patterns for the $Bi_4V_2O_{10}$ material taken along the (a) [100] and (b) [$\bar{1}$10] zone axes.

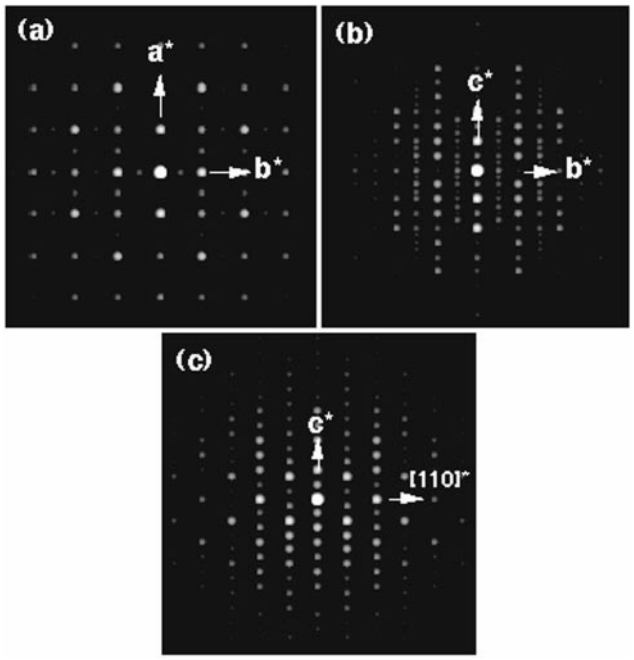

Fig. 5 Calculated electron diffraction patterns for $Bi_4V_2O_{11}$ using the atomic coordinates of space group $P22_12_1$ in the (a) [001], (b) [100] and (c) [$\bar{1}$10] reciprocal projections.

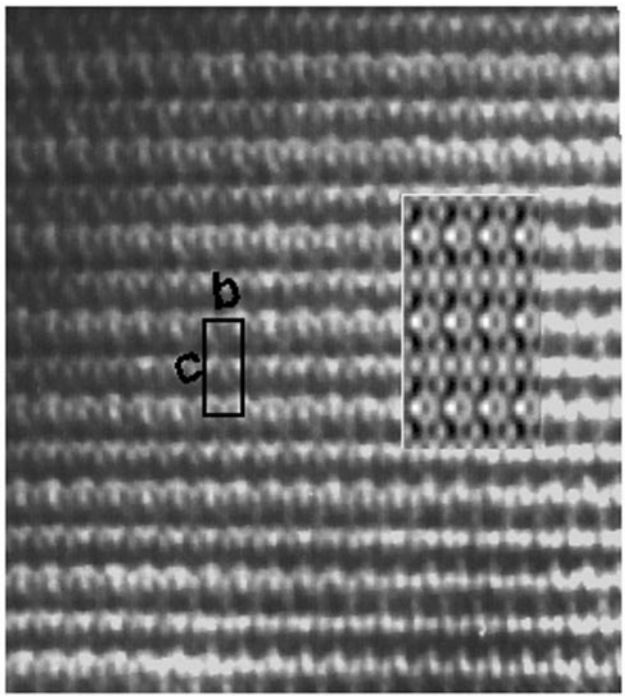

Fig. 6 HREM image for $Bi_4V_2O_{10}$ in the [100] projection. Corresponding calculated image shown as inset (conditions: $\Delta f = -60$ nm, $t = 7.0$ nm) (atomic coordinates of space group $P22_12_1$ used as input data).

Acknowledgements

We are grateful to the Centro de Microscopía Electrónica (UCM) for facilities. We acnowledge the financial support of CICYT (Spain) through project no. MAT98-0648.

References

1 B. Aurivillius, *Ark. Kemi.*, 1949, **1**, 463; B. Aurivillius, *Ark. Kemi.*, 1949, **1**, 499; B. Aurivillius, *Ark. Kemi.*, 1950, **2**, 519.

2 K. R. Kendall, C. Navas, J. K. Thomas and H. C. Zur Loye, *Chem. Mater.*, 1996, **8**, 642 and references therein.
3 F. Abraham, M. F. Debreuille-Gresse, G. Mairesse and G. Nowogrocki, *Solid State Ionics*, 1988, **28–30**, 529.
4 F. Abraham, J. C. Boivin, G. Mairesse and G. Nowogrocki, *Solid State Ionics*, 1990, **40/41**, 934.
5 J. Galy, R. Enjalbert, P. Millán and A. Castro, *C. R. Acad. Sci., Ser. II*, 1993, **317**, 43.
6 O. Joubert, A. Jouanneaux and M. Ganne, *Nucl. Instrum. Methods Phys. Res., Sect. B*, 1995, **97**, 119.
7 S. Sorokina, R. Enjalbert, P. Baules, A. Castro and J. Galy, *J. Solid State Chem.*, 1996, **125**, 54.
8 C. Satto, P. Millet, P. Sciau, C. Roucau and J. Galy, *Mater. Res. Bull.*, 1999, **34**, 655.
9 M. Huvé, R. N. Vannier, G. Nowogrocki, G. Mairesse and G. Van Tendeloo, *J. Mater. Chem.*, 1996, **6**, 1339.
10 K. B. R. Varma, G. N. Subbana, T. N. Guru Row and C. N. R. Rao, *J. Mater. Res.*, 1990, **5**, 2718.
11 O. Joubert, A. Jouanneaux and M. Ganne, *Mater. Res. Bull.*, 1994, **29**, 175.
12 R. Killas, MacTempas 1.7.2, HRTEM Image Simulation Software, Total Resolution, Inc., Berkeley, CA, USA.